










Climate Evaluation of a High-Resolution Regional Model over the Canary Current Upwelling System

Ruben Vazquez¹ , Ivan Parras-Berrocal¹ , William Cabos² ,
Dmitry V. Sein³ , Rafael Mañanes¹ , Juan I. Perez² ,
and Alfredo Izquierdo¹ 

¹ University of Cadiz, 11510 Cadiz, Spain
{ruben.vazquez, ivan.parras, rafael.salinas,
alfredo.izquierdo}@uca.es

² University of Alcalá, 28801 Alcalá de Henares, Spain
{william.cabos, nacho.perez}@uah.es

³ Alfred Wegener Institute for Polar and Marine Research,
27570 Bremerhaven, Germany
dmitry.sein@awi.de

Abstract. Coastal upwelling systems are very important from the socio-economic point of view due to their high productivity, but they are also vulnerable under changing climate. The impact of climate change on the Canary Current Upwelling System (CCUS) has been studied in recent years by different authors. However, these studies show contradictory results on the question whether coastal upwelling will be more intense or weak in the next decades. One of the reasons for this uncertainty is the low resolution of climate models, making it difficult to properly resolve coastal zone processes. To solve this issue, we propose the use of a high-resolution regional climate coupled model. In this work we evaluate the performance of the regional climate coupled model ROM (REMO-OASIS-MPIOM) in the influence zone of the CCUS as a first step towards a regional climate change scenario downscaling. The results were compared to the output of the global Max Planck Institute Earth System Model (MPI-ESM) showing a significant improvement.

Keywords: ROM · Canary current · Regional climate modelling

1 Introduction

The Eastern Boundary Upwelling Systems (EBUSs) are highly productive coastal ocean areas where cold water upwells by the action of favourable winds [1]. The upwelling is associated to the along-shore Trade winds dominating these subtropical regions and causing Ekman transport from the coast to the open ocean. There are four EBUSs, being the Canary Current Upwelling System (CCUS) one of the most important fishery grounds in the world [2]. The Canary current is part of the North Atlantic subtropical gyre, extending from the northern tip of the Iberian Peninsula at (43°N) to the south of Senegal at about 10°N (Fig. 1).

The CCUS has a seasonal variability related to that of the Trade winds and the Intertropical Convergence Zone (ITCZ) migration (Fig. 1). At the Iberian coast the CCUS presents a marked seasonal cycle with the upwelling season beginning in spring and extending through summer and early autumn, and downwelling events frequently observed during wind relaxations in winter [3]. The length of the upwelling season increases progressively as latitude decreases, with upwelling becoming mostly a year-round phenomenon at tropical–subtropical latitudes [4].

In the last decades many authors have studied the EBUEs due to their vulnerability under global warming conditions. Bakun [5] hypothesized that the increase in the ocean–land thermal gradient due to greenhouse warming would result in stronger along-shore winds intensifying the upwelling of deeper water to the surface.

Sydeman et al. [6], through a meta-analysis of the existing literature on upwelling-favourable wind intensification, revealed contradictory results between observational data and model-data reanalysis. Their results showed equivocal wind intensification in the Canary upwelling, in agreement with the analysis of Varela et al. [7], which also highlighted the importance of high resolution wind database to properly resolve conditions at the scale of coastal upwelling in intense and localized upwelling zones.

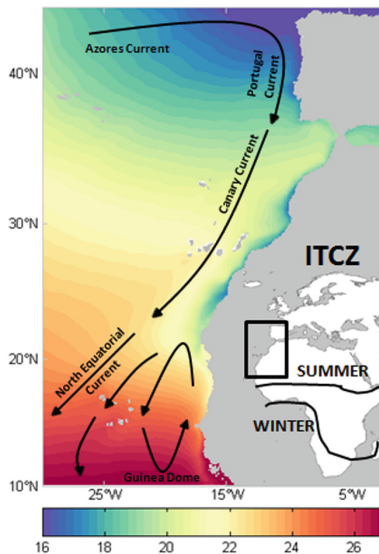


Fig. 1. Sea surface temperature ($^{\circ}\text{C}$) and upper ocean circulation in the Canary current system. Also it is showed the seasonal migration of the ITCZ (based on Benazzouz et al. [8]).

Thus we present and validate the performance of a high-resolution regionally coupled atmosphere ocean model in the CCUS, so the advantages of this modelling approach can be assessed, and the uncertainty in the assessment of upwelling-favourable wind intensification at the CCUS under global warming reduced.

2 Models and Data Sets

The regionally coupled climate model ROM [9] comprises the REgional atmosphere MOdel (REMO), the Max Planck Institute Ocean Model (MPI-OM), the HAMBurg Ocean Carbon Cycle (HAMOCC) model, the Hydrological Discharge (HD) model, the soil model [10] and dynamic/thermodynamic sea ice model [11] which are coupled via OASIS [12] coupler, and was called ROM by the initials REMO-OASIS-MPIOM. The regional downscaling allows the interaction of atmosphere and ocean in the region covered by REMO (Fig. 2a), while the rest of the global ocean is driven by energy, momentum and mass fluxes from global atmospheric data used as external forcing.

The oceanic component of ROM is the Max Planck Institute Ocean Model (MPI-OM) developed at the Max Planck Institute for Meteorology (Hamburg, Germany) [13, 14]. The MPI-OM configuration used for all experiments features the grid poles over North America and Northwestern Africa (Fig. 2a). The horizontal resolution ranges from 5 km (close to the NW African coast) to 100 km in the southern oceans (Fig. 2b). This feature allows a local high resolution in the region of interest allowing the study of local-scale processes while maintaining a global domain (e.g. Izquierdo and Mikolajewicz [15]).

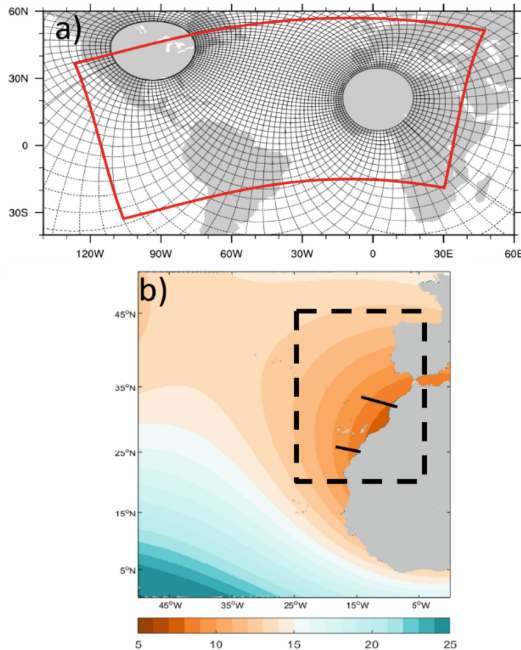


Fig. 2. (a) Atmosphere and ocean ROM grids. MPI-OM variable resolution grid (black lines, drawn every twelfth), REMO domain (red line). (b) MPI-OM grid resolution (km) in the Canary current system. Localization of the study zone (dashed black line) and of the 2 chosen transects (solid black lines). (Color figure online)

The atmospheric component of ROM is the REgional atmosphere MOdel (REMO) [16]. The dynamic core of the model as well as the discretization in space and time are based on the Europa-Model of the Germany Weather service [17]. The physical parameterizations are taken from the global climate model ECHAM versions 4 and 5 [18, 19]. To avoid the largely different extensions of the grid cells close to the poles, REMO uses a rotated grid, with the equator of the rotated system in the middle of the model domain with a constant resolution of 25 km [9].

ROM was compared with the Max Plank Institute for Meteorology – Earth System Model (MPI-ESM) to analyze the differences between a regional and global model. The MPI-ESM has been used in the context of the CMIP5 process (Coupled Models Intercomparison Project Phase 5) and consists of the coupled general circulation models for the atmosphere (ECHAM6) and the ocean (MPI-OM) and the subsystem models for land and vegetation JSBACH [20, 21] and for the marine biogeochemistry HAMOCC5 [22].

The MPI-ESM has been developed for a variety of configurations differing in the resolution of ECHAM6 or MPI-OM (MPI-ESM-LR, -MR). The low resolution (LR) configuration uses for the ocean a bipolar grid with 1.5° resolution and the medium resolution (MR) decreases the horizontal grid spacing of the ocean to 0.4° with a tripolar grid, two poles localized in Siberia and Canada and a third pole at the South Pole [23]. The experiments used for the evaluation and the analyses were the historical run and the RCP4.5 scenario.

Table 1. Observational data products used in the ROM validation.

Product	Description
OSTIA	Global high-resolution (6 km) SST from the Operational Sea Surface Temperature and Sea Ice Analysis (OSTIA) [24]. The temporal resolution is daily from April 2006 to the present
SCOW	Scatterometer Climatology of Ocean Winds (SCOW) based on 8 years (September 1999 to August 2007) of QuikSCAT data. It provides a monthly wind stress climatology with 1/4° resolution [25]
WOA18	The World Ocean Atlas 2018 (WOA18) is a set of objectively analyzed (1° grid) climatological fields of in situ temperature, salinity, dissolved oxygen, nutrients, ... [26]
WOD	The World Ocean Database (WOD) includes in situ measurements of temperature, salinity, dissolved oxygen and nutrients from 1773 to the present [27]

Finally, the different datasets used in the present paper to evaluate and analyze ROM are described in the Table 1. OSTIA (the system uses data from a combination of infrared and microwave satellites as well as in situ data) appears to be one of the best options with respect to other available reanalysis data for mesoscale processes [28].

3 Results

3.1 Sea Surface Temperature

ROM Sea Surface Temperature (SST) was evaluated using OSTIA in the period 2008–2012. In addition, ROM output was compared to MPI-ESM-LR and MR (Fig. 3).

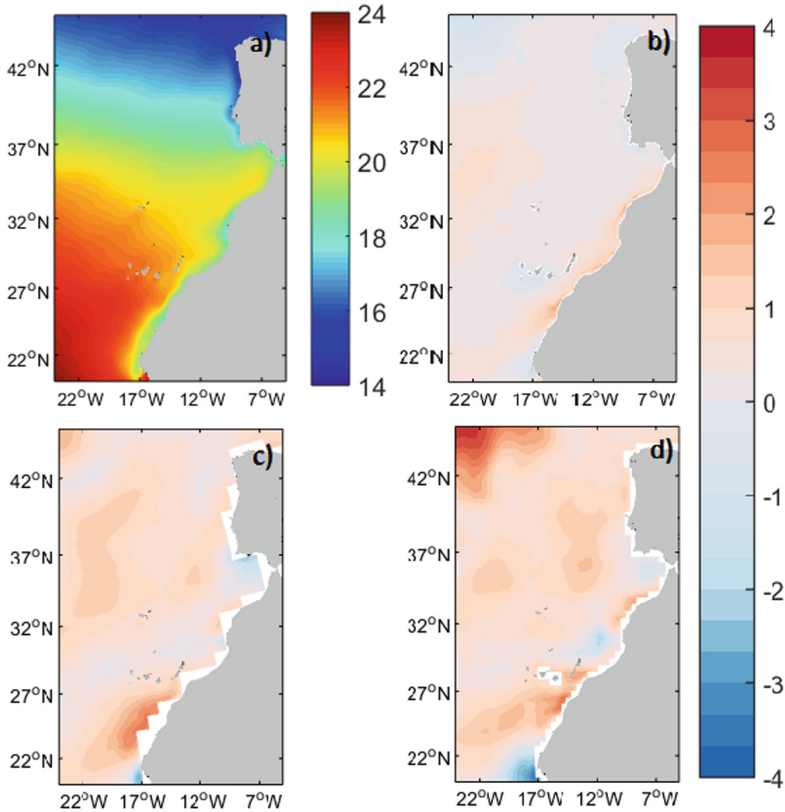


Fig. 3. Mean SST ($^{\circ}\text{C}$): (a) OSTIA and differences with ROM (b), MPI-ESM-LR (c) and MPI-ESM-MR (d) for 2008–2012.

Mean SST 2008–2012

The time averaged SST in OSTIA (Fig. 3a) shows a clear meridional gradient with lower SST by the coast as a result of the upwelled waters.

Comparison to model SSTs shows that, although all three reproduce the general OSTIA SST pattern reasonably well, ROM clearly outperforms MPI-ESM, attaining smaller differences (Fig. 3b–d). This is more remarkably close to the coast, where ROM higher resolution plays a role.

It allows ROM to properly reproduce some smaller scale features in the field of SST lacking in the MPI-ESMs, notably along the Iberian coast and by the Strait of Gibraltar. However, we can observe a cold bias along the coast in ROM from the Strait of Gibraltar to Cape Blanc (from 35°N to 22°N). This is evident in Fig. 4a, plotting the SST of the grid-point closest to the coast from 20°N to 42°N for all four datasets.

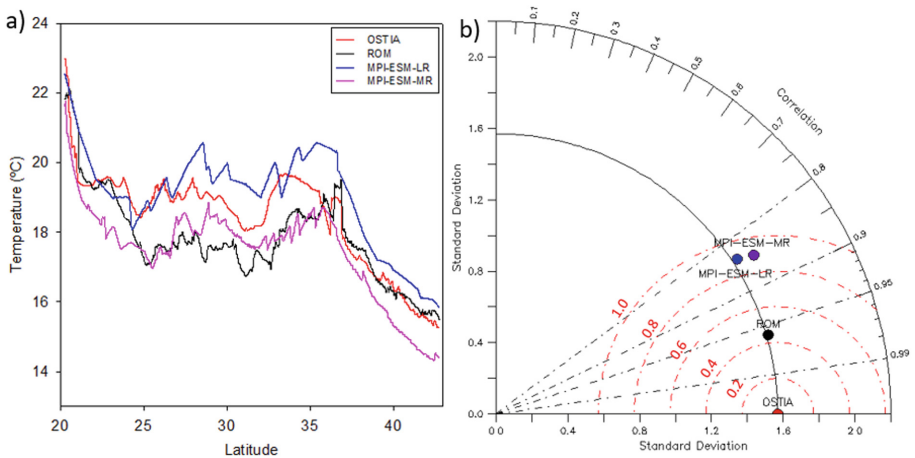


Fig. 4. (a) Meridional distribution of SST in the ocean grid-point closest to the coast. (b) Taylor Diagram for the CCUS region SST during 2008–2012 period. The diagram summarizes the relationship between standard deviation (°C), correlation (r) and RMSE (red lines, °C) among all datasets. (Color figure online)

The model performance in the CCUS was evaluated by means of a Taylor diagram (Fig. 4b) averaging SST over the box enclosed by 22°N to 45°N and 5°W to 25°W. The SST temporal variability, expressed by the standard deviation, is similar in all datasets, with a value around 1.6 °C. However, when comparing the models output to analysis data (OSTIA) ROM clearly improves both MPI-ESM configurations, showing a higher correlation coefficient (0.96 vs 0.85) and a lower RMSE (0.4 °C vs 1.0 °C). Despite differences in horizontal resolution, MPI-ESM-LR and MPI-ESM-MR show a very similar performance.

Seasonal Cycle

The CCUS experiences an important seasonal cycle in SST characterized by the winter (DJF) and summer (JJA) SSTs. Figure 5 shows SST differences between OSTIA and the models output (ROM, MPI-ESM-LR, and MPI-ESM-MR). ROM biases are lower than in any of the MPI-ESM configurations, and generally within ± 1 °C, notably improving a JJA warm bias in the SW Iberian margin and a cold bias south of Canary Islands.

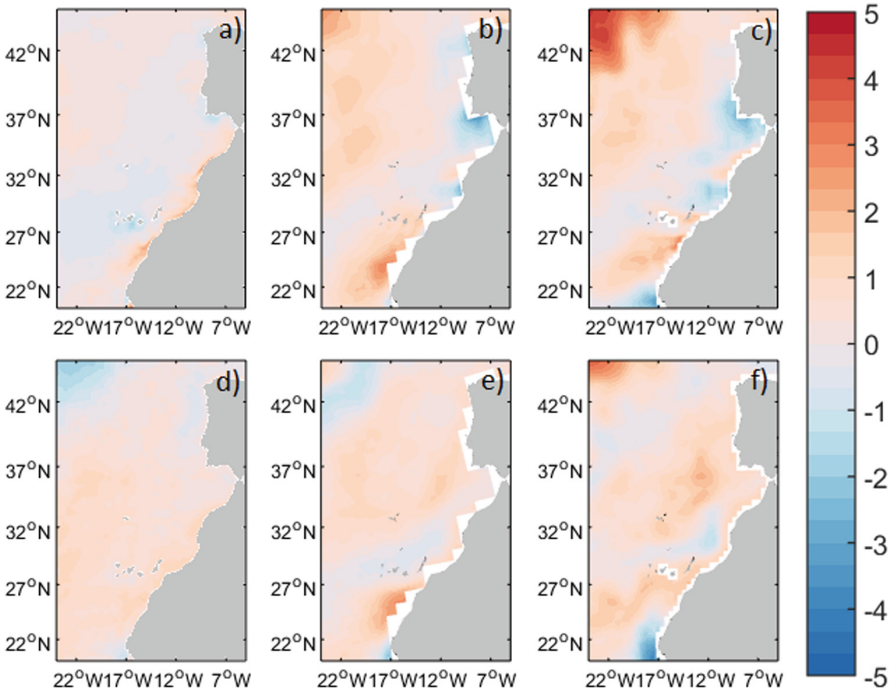


Fig. 5. OSTIA SST (°C) difference with ROM (a), MPI-ESM-LR (b) and MR (c) in summer (JJA); and ROM (d), MPI-ESM-LR (e) and MR in winter (DJF)

Table 2 shows the seasonal statistics comparing model SST values in the defined CCUS box with OSTIA analysis. All models perform better (according to correlation coefficient and RMSE) in winter. However even in summer ROM presents a high correlation of 0.93, while correlation for MPI-ESM-LR and MR drastically drops down to 0.69 and 0.72, respectively. Analogous situation takes place for RMSE, with ROM showing always better results than MPI-ESM configurations.

Table 2. Seasonal statistics comparing OSTIA and model SST

	Winter			Summer		
	r	RMSE (°C)	Sd (°C)	r	RMSE (°C)	Sd (°C)
ROM	0.98	0.38	1.60	0.93	0.56	1.49
MPI-ESM-MR	0.92	0.78	1.99	0.72	0.94	1.25
MPI-ESM-LR	0.91	0.78	1.87	0.69	0.97	1.20
OSTIA			1.79			1.26

3.2 Wind Stress

The ROM surface wind stress was evaluated with the Scatterometer Climatology of Ocean Winds (SCOW) comprising QuikSCAT observations from 1999 to 2007.

Figure 6 presents the time averaged (1999–2007) zonal and meridional components of wind stress corresponding to SCOW, ROM, MPI-ESM-LR and MPI-ESM-MR. The zonal component of wind stress shows a similar spatial pattern for all datasets, with a change of sign around 36°N , but ROM presents smaller biases than the MPI-ESM. SCOW and ROM fields of the meridional component of wind stress are very similar, both showing local maxima south of Cap Ghir and Cape Blanc. MPI-ESM-LR properly reproduces the general pattern, but not the smaller scale details. Remarkably, MPI-ESM-MR shows a different pattern, with northern winds predominating north 37°N .

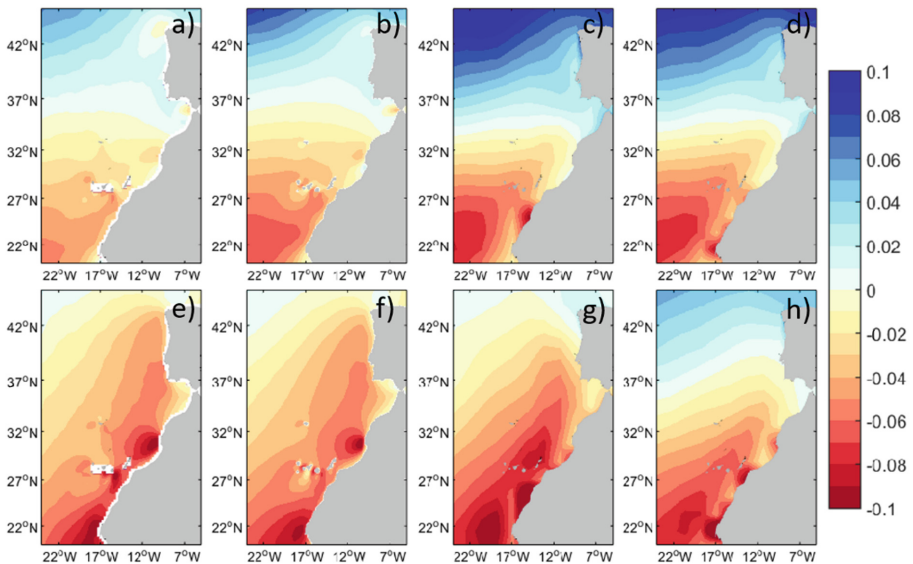


Fig. 6. Zonal component of wind stress (N/m^2) from SCOW (a), ROM (b), MPI-ESM-LR (c) and MPI-ESM-MR (d). Meridional component of the wind stress (N/m^2) from SCOW (e), ROM (f), MPI-ESM-LR (g) and MPI-ESM-MR (h).

3.3 Thermal Vertical Structure

The thermal vertical structure of the upper 200 m from ROM was compared with the climatology World Ocean Atlas 2018 (WOA18) [26] and with the historical in-situ data from the World Ocean Database (WOD) [27]. The analysis was realized through two across-shore transects at Cape Ghir and to the south of the Canary Islands (Cape Bojador). In the comparison we used 12 available CTD/XBT stations for Cape Ghir transect and 21 for Cape Bojador. All the observations were taken in summer periods between 1985 and 2004.

WOD observations show a clear thermal stratification at both transects (Figs. 7a and b) with temperatures ranging from 14 °C at 200 m depth to 24 °C at the surface, and somewhat colder at Cape Ghir than at Cape Bojador. ROM temperature transects properly reproduce this structure (Figs. 7c and d), but limiting the extension of colder waters (≈ 14 °C) to the coast, and showing a small warm bias at depth. Interestingly, when compared to direct observations WOA18 (Figs. 7e and f) shows a larger warm bias than ROM, which is more evident near the coast. This is a clear evidence that the higher horizontal resolution of ROM allows to reproduce smaller scale processes that are partly masked in the climatology.

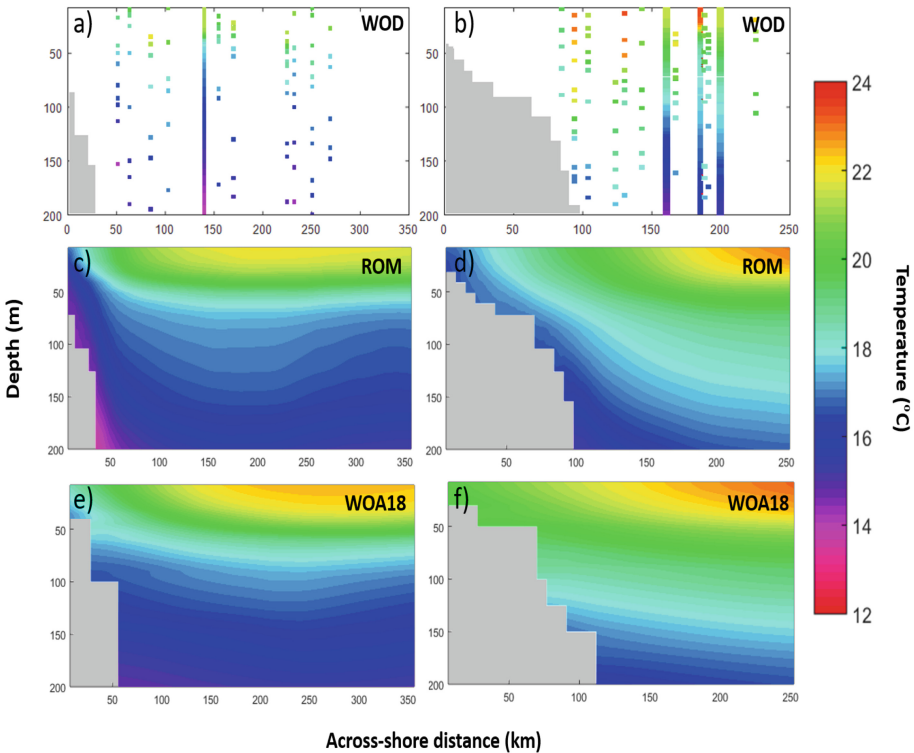


Fig. 7. Temperature (°C) transects at Cape Ghir (a, c, e) and Cape Bojador (b, d, f) for summers periods between 1985 and 2004. Transect referred to in Fig. 2.

To clearly show the differences near coast Fig. 8 plots the temperature profiles corresponding to the location of the nearest to coast observations from WOD. In the first vertical profile localized at Cape Ghir (Fig. 8a), we can observe a similar temperature profiles for the three datasets in the upper 100 m, deeper the temperature profiles start to diverge, being the warm bias larger in WOA18 than in ROM.

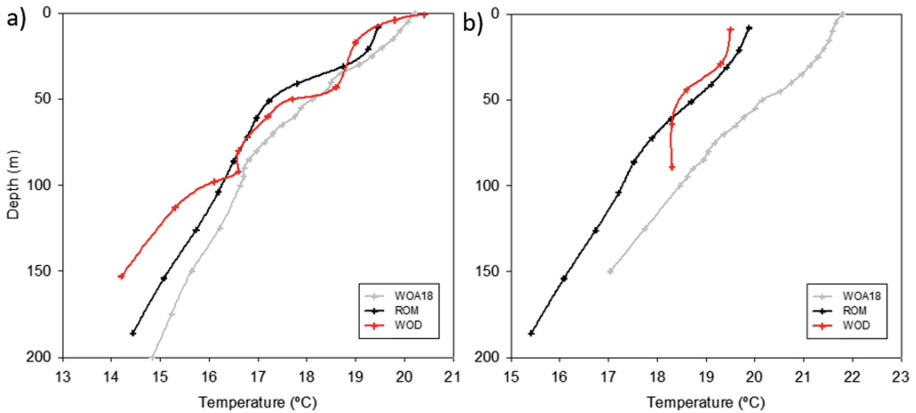


Fig. 8. Temperature (°C) profile at Cape Ghir (a) and Cape Bojador (b) in 1985–2004 summer period.

The WOD Cape Bojador profile (Fig. 9b) is much shallower, however at surface WOA18 is 2 °C warmer than WOD and ROM.

4 Discussion and Conclusions

In this study, the regional atmosphere-ocean model coupled was validated for the CCUS region. The ROM ocean outputs analyzed were SST, surface wind stress and thermal vertical structure.

ROM time mean and seasonal SST was validated against OSTIA data set, showing biases largely bounded to ± 1 °C, correlations coefficients above 0.9 and RMSE below 0.4 °C. All the statistics showed a better performance than MPI-ESM-LR and MPI-ESM-MR. Interestingly, between both MPI-ESM configurations there was almost no improvements, which is an indication that ROM is not only providing a better result due to its higher resolution, but also because it is able of better reproducing mesoscale coastal processes. ROM also presented cold biases along the North African coast stronger in summer periods. Li et al. [29] regional model for the California upwelling showed a similar cold bias when compared to satellite data. Mason et al. [30] reported a similar bias in their ROMS model for the Canary upwelling, and blamed the uncertainty in the nearshore model wind structure. However, that bias can also be a consequence of the analysis system used in OSTIA since it assumes that the observation errors are not locally biased. OSTIA corrects the observation errors in a global way [24], therefore in zones with intense mesoscale dynamics, like the coastal strip along the CCUS, it could generate biases.

Other important variable to evaluate in the CCUS is the surface wind stress. ROM surface wind stress was compared to SCOW, showing small differences. The biases found did not exceed 0.006 N/m². Taylor diagrams for SCOW and model wind stress components averaged over the CCUS box (Fig. 9) show the better performance of ROM as compared to MPI-ESM configurations and again, this improvement is not only

related to a better resolution, as meridional wind stress is worse in MPI-ESM-MR than in MPI-ESM-LR.

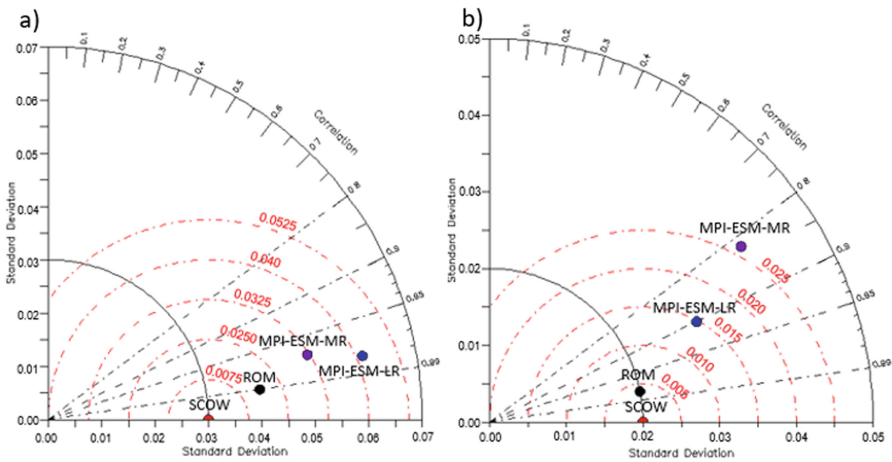


Fig. 9. Taylor diagrams for CCUS zonal (a) and meridional (b) surface wind stress components during 1999–2009 period.

ROM simulated wind stress was clearly better than MPI-ESM, pointing out to the need of regional downscaling to properly simulate the CCUS dynamics.

The analysis of the vertical thermal structure in two across-shore transects also showed that ROM is able to reproduce near coast temperature gradients, likely masked if the resolution is not very high.

In conclusion, ROM shows clear improvements in reproducing the surface wind and ocean temperature fields in the CCUS when compared to global climate models as MPI-ESM. The improvement is related to a much higher horizontal resolution in the atmosphere and in the ocean, which allows to better simulate the dominant mesoscale coastal dynamics at the CCUS. The results here give ground to the future use of ROM to have deeper insight into the state changes expected to happen at CCUS by the end of 21st century.

Acknowledgement. This work has been developed within the framework of the European Cooperation Project Interreg VA España-Portugal “OCASO” (Southwest Coastal Environmental Observatory,0223_OCASO_5_E).

References

1. Tim, N., Zorita, E., Hünicke, B., Yi, X., Emeis, K.-C.: The importance of external climate forcing for the variability and trends of coastal upwelling in past and future climate. *Ocean Sci.* **12**, 807–823 (2016). <https://doi.org/10.5194/os-12-807-2016>
2. Hagen, E., Feistel, R., Agenbag, J.J., Ohde, T.: Seasonal and interannual changes in intense Benguela upwelling (1982–1999). *Oceanol. Acta* **24**(6), 557–568 (2001). [https://doi.org/10.1016/S0399-1784\(01\)01173-2](https://doi.org/10.1016/S0399-1784(01)01173-2)

3. Cordeiro, N., Dubert, J., Nolasco, R., Barton, E.D.: Transient response of the Northwestern Iberian upwelling regime *PLoS ONE* **13**(5) (2018). <https://doi.org/10.1371/journal.pone.0197627>
4. Wang, D.W., Gouhier, T.C., Menge, B.A., Ganguly, A.R.: Intensification and spatial homogenization of coastal upwelling under climate change. *Nature* **518** (2015). <https://doi.org/10.1038/nature14235>
5. Bakun, A.: Global climate change and intensification of coastal ocean upwelling. *Science* **247**, 198–201 (1990). <https://doi.org/10.1126/science.247.4939.198>
6. Sydeman, W.J., et al.: Climate change and wind intensification in coastal upwelling ecosystems. *Science* **345**, 77–80 (2014). <https://doi.org/10.1126/science.1251635>
7. Varela, R., Alvarez, I., Santos, F., deCastro, M., Gomez-Gesteira, M.: Has upwelling strengthened along worldwide coasts over 1982–2010? *Sci. Rep.* **5** (2015). <https://doi.org/10.1038/srep10016>
8. Benazzouz, A., et al.: An improved coastal upwelling index from sea surface temperature using satellite-based approach – the case of the Canary current upwelling system. *Cont. Shelf Res.* **81**, 38–54 (2014). <https://doi.org/10.1016/j.csr.2014.03.012>
9. Sein, D.V., et al.: Regionally coupled atmosphere-ocean-sea ice marine biogeochemistry model ROM: 1. Description and validation. *J. Adv. Model. Earth Syst.* **7**, 268–304 (2015). <https://doi.org/10.1002/2014ms000357>
10. Rechid, D., Jacob, D.: Influence of monthly varying vegetation on the simulated climate in Europe. *Meteorol. Z.* **15**, 99–116 (2006). <https://doi.org/10.1127/0941-2948/2006/0091>
11. Hibler III, W.D.: A dynamic thermodynamic sea ice model. *J. Phys. Oceanogr.* **9**, 815–846 (1979). [https://doi.org/10.1175/1520-0485\(1979\)009<0815:adtsim>2.0.co;2](https://doi.org/10.1175/1520-0485(1979)009<0815:adtsim>2.0.co;2)
12. Valcke, S.: The OASIS3 coupler: a European climate modelling community software. *Geosci. Model Dev.* **6**, 373–388 (2013). <https://doi.org/10.5194/gmd-6-373-2013>
13. Marsland, S.J., Haak, H., Jungclaus, J.H., Latif, M., Roeske, F.: The Max-Planck - Institute global ocean/sea ice model with orthogonal curvilinear coordinates. *Ocean Model.* **5**(2), 91–127 (2003). [https://doi.org/10.1016/S1463-5003\(02\)00015-X](https://doi.org/10.1016/S1463-5003(02)00015-X)
14. Jungclaus, J.H., et al.: Characteristics of the ocean simulations in MPIOM, the ocean component of the MPI-Earth system model. *J. Adv. Model Earth Syst.* **5**, 422–446 (2013). <https://doi.org/10.1002/jame.20023>
15. Izquierdo, A., Mikolajewicz, U.: The role of tides in the spreading of mediterranean outflow waters along the southwestern Iberian margin. *Ocean Model.* **133**, 27–43 (2019). <https://doi.org/10.1016/j.ocemod.2018.08.003>
16. Jacob, D.: A note to the simulation of the annual and interannual variability of the water budget over the Baltic Sea drainage basin. *Meteorol. Atmos. Phys.* **77**(1–4), 61–73 (2001). <https://doi.org/10.1007/s007030170017>
17. Majewski, D.: The Europa modell of the Deutscher Wetterdienst. In: Seminar Proceedings ECMWF, vols. 2, 5, pp. 147–191. ECMWF, Reading (1991)
18. Roeckner, E., et al.: The atmospheric general circulation model ECHAM-4: model description and simulation of present-day-climate. Report 218, MPI für Meteorol., Hamburg, Germany (1996)
19. Roeckner, E., et al.: The atmospheric general circulation model ECHAM 5. PART I: model description. Report 349, MPI für Meteorol., Hamburg, Germany (2003)
20. Reick, C.H., Raddatz, T., Brovkin, V., Gayler, V.: The representation of natural and anthropogenic land cover change in MPIESM. *J. Adv. Model. Earth Syst.* **5**, 1–24 (2013). <https://doi.org/10.1002/jame.20022>
21. Schneck, R., Reick, C.H., Raddatz, T.: The land contribution to natural CO₂ variability on time scales of centuries. *J. Adv. Model. Earth Syst.* **5**, 354–365 (2013). <https://doi.org/10.1002/jame.20029>

22. Ilyina, T., Six, K., Segschneider, J., Maier-Reimer, E., Li, H., Nunez-Riboni, I.: Global ocean biogeochemistry model HAMOCC: model architecture and performance as component of the MPI-Earth system model in different CMIP5 experimental realizations. *J. Adv. Model. Earth Syst.* (2013). <https://doi.org/10.1029/2012ms000178>
23. Giorgetta, M.A., et al.: Climate and carbon cycle changes from 1850 to 2100 in MPI-ESM simulations for the coupled model intercomparison project phase 5. *J. Adv. Model. Earth Syst.* **5**, 572–597 (2013). <https://doi.org/10.1002/jame.20038>
24. Stark, J.D., Donlon, C.J., Martin, M.J., McCulloch, M.E.: OSTIA: an operational, high resolution, real time, global sea surface temperature analysis system. In: *OCEANS 2007—Europe*, pp. 1–4 (2007). <https://doi.org/10.1109/oceanse.2007.4302251>
25. Risien, C.M., Chelton, D.B.: A global climatology of surface wind and wind stress fields from eight years of QuikSCAT Scatterometer data. *J. Phys. Oceanogr.* **38**, 2379–2413 (2008). <https://doi.org/10.1175/2008JPO3881.1>
26. Locarnini, R.A., et al.: *World Ocean Atlas 2018: Temperature*. A. Mishonov Technical Ed. vol. 1 (2018, in preparation)
27. Boyer, T.P., et al.: *World Ocean Database 2018* (2018, in preparation)
28. Desbiolles, F., et al.: Upscaling impact of wind/sea surface temperature mesoscale interactions on Southern Africa austral summer climate. *Int. J. Climatol.* **38**(12), 4651–4660 (2018). <https://doi.org/10.1002/joc.5726>
29. Li, H., Kanamitsu, M., Hong, S.Y.: California reanalysis downscaling at 10 km using an ocean-atmosphere coupled regional model system. *J. Geophys. Res. Atmos.* **117**, D12 (2012). <https://doi.org/10.1029/2011jd017372>
30. Mason, E., et al.: Seasonal variability of the Canary current: a numerical study. *J. Geophys. Res. Oceans* **116**(C6) (2011). <https://doi.org/10.1029/2010jc006665>